Precision Engineering 34 (2010) 164–170

Contents lists available at ScienceDirect

Precision Engineering

journal homepage: www.elsevier.com/locate/precision

Optimization and temperature mapping of an ultra-high thermal stability environmental enclosure

Yong Zhao [a], David L. Trumper [b], Ralf K. Heilmann [a], Mark L. Schattenburg [a,*]

[a] Space Nanotechnology Laboratory, Massachusetts Institute of Technology, Cambridge, MA 02139, United States
[b] Precision Motion Control Laboratory, Massachusetts Institute of Technology, Cambridge, MA 02139, United States

ARTICLE INFO

Article history:
Received 27 September 2007
Received in revised form 16 March 2009
Accepted 27 May 2009
Available online 12 June 2009

Keywords:
High-stability thermal control
Lead control
Temperature measurement
Temperature gradients
Environmental enclosure

ABSTRACT

Precision metrology, lithography and machining systems will soon require sub-nanometer tolerances in order to meet the evolving needs of industry. This, in turn, requires thermal control of large environmental enclosures with sub-millidegree single-point stability and control of temperature gradients to several millidegrees. In order to optimize the system's thermal controls, it is essential to measure the open-loop transfer function. We report a technique that obtains the open-loop transfer function by utilizing a dynamic signal analyzer to perform a closed-loop frequency response measurement of the thermal system. Based on the transfer function, we designed a PI-lead compensation controller and achieved one-sigma air temperature stability of less than 1 m°C at a single point over 2 h. In order to rapidly map temperature gradients over large regions inside the 7 m^3-volume enclosure, we have developed a measurement scheme that involves mechanically scanning a network of thermistors. Accurate cross calibration of the thermistors and a study of self-heating effects on temperature measurement in moving air have also been performed, which assures the relative accuracy of the thermistors is less than 1 m°C. Comparing temperature gradient maps taken before and after control improvements shows improved temperature stability over the mapped volumes.

1. Introduction

Thermal control of environmental enclosures is becoming increasingly critical as precision metrology, lithography and machining systems require sub-nanometer tolerances. The primary deleterious effects of air temperature fluctuations on tool precision are errors in interferometer beam paths and the thermal expansion of the workpiece and metrology frame. According to the updated Edlen equation for the refractive index of air with $\lambda = 633.0$ nm [1], for the laboratory conditions of one atmosphere pressure (101.325 kPa), 50% relative humidity, and temperatures close to 20 °C, the linear approximation of the air refractive index, n, with respect to temperature, T, in degrees centigrade is

$$n = 1 + 2.7137403 \times 10^{-4} - 9.2984 \times 10^{-7} \times T. \quad (1)$$

For example, thermal control within ±0.01 °C, which is typical for state-of-the-art equipment, will cause a change of ±9.3 ppb in the refractive index of air. This change will result in a ±2.8 nm stage interferometer error for 300 mm stage translation. For a 300 mm wafer chuck, ±0.01 °C thermal control will cause a ±1.8 nm thermal expansion error for a super-Invar chuck and a ±0.16 nm thermal expansion error for a Zerodur chuck. For the same geometry and environmental conditions, improved thermal control to within ±0.001 °C (1 m°C) can reduce the stage interferometer error to ±0.28 nm and the thermal expansion error to ±0.18 nm for a super-invar chuck and ±0.016 nm for a Zerodur chuck.

Some thermal control systems have achieved temperature stability of millidegrees or better by using air-flow standard cell enclosures [2,3] or enclosures utilizing flowing water as the thermal control medium [4]. Within large-volume air-flow enclosures, one-sigma air temperature stability of 2–3 m°C at a single point has been demonstrated [5,6]. In this paper we report a technique for improving the thermal control of an environmental enclosure designed for a precision lithography tool [6–8] to drive the single-point one-sigma temperature stability down to sub-millidegree levels. In addition to the thermal control at a single point, we have developed a method for rapidly monitoring and mapping temperature gradients over critical areas inside the environmental enclosure.

Our environmental enclosure (see Fig. 1a), whose internal dimensions are approximately 2.0-m long × 1.7-m wide × 2.1-m high, consists of two identical air handler units [6]. As shown in Fig. 1b, in each unit thermally controlled air is forced into the chamber in the center through 1.1-m by 0.56-m ULPA filters and returns through grills located at the top and bottom of the chamber. The air leaves the filters in laminar flow with velocity of approximately

* Corresponding author at: 70 Vassar Street, 37-487, Cambridge, MA, 02139, United States. Tel.: +1 617 253 3180; fax: +1 617 452 2888.
E-mail address: marks@space.mit.edu (M.L. Schattenburg).

0141-6359/$ – see front matter © 2009 Elsevier Inc. All rights reserved.
doi:10.1016/j.precisioneng.2009.05.006

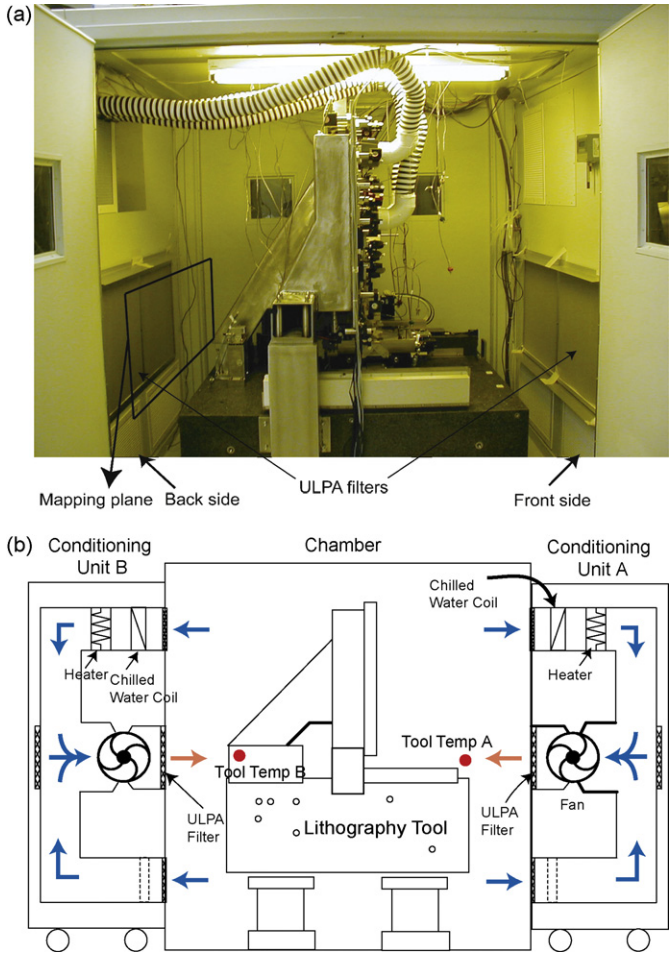

Fig. 1. The environmental enclosure. (a) Photograph of the inside of the enclosure, which houses a scanning interference lithography tool. Temperature-controlled air leaves the ULPA filters and is directed towards the critical volume of the tool at the center. (b) Schematic of the enclosure showing air paths and temperature measurement points.

1 m/s and is situated to bathe the critical volume of the lithography tool, which contains the interferometer beam paths and the work piece, with well-conditioned air from both sides. The horizontal flow design minimizes the controlled volume of air and potential influx of heated air from stage motors and active elements in the optical bench. The air returned through the top grill is cooled by a chilled water coil (water temperature ~8 °C) and then reheated by fast electrical heaters to a controlled temperature. The water temperature was selected to efficiently pull heat, which is generated by fan motors, stage motors and electronics, out of the recirculated air, and also allows some head room for the fast heaters, which can add but cannot subtract heat from the air-flow. The 8 °C water has the additional benefit of drying the air down to a 45.9% RH. Since laboratory air, which is introduced into the enclosure as a small amount of make-up, is typically controlled to 47 ± 9% RH, the chill coil results in a well controlled humidity without large positive excursions which can occur in the summer months.

After mixing with the bottom return air, the reheated air is forced by a fan through a mixing chamber to enter the chamber. The total air volume of the chamber, after accounting for the volume occupied by the lithography tool, is ~6 m^3. The high air velocity results in a chamber air change-over time of ~10 s. The thermal sensors (Deban Air010 thermistors) in each unit for the feedback thermal control are located in front of the filter planes (see Tool Temp A and B in Fig. 1b).

2. Measuring the transfer function

Measuring a system's open-loop transfer function is a critical step during development of controls to achieve the desired performance. However, sometimes it is impossible to take a direct open-loop transfer function measurement because of noise issues or field-test limitations. Alternatively, we can calculate the transfer function based on closed-loop frequency response measurements. As shown in Fig. 2, we used a HP 35670A Dynamic Signal Analyzer to inject a swept-sine stimulus signal, *N*, into the loop. Frequency response measurements were then taken at points Y_1 and Y_2, which were tapped off of the heater control circuitry. The open-loop transfer function, *GTH*, of this thermal system is calculated from the measurements using equations

$$\begin{cases} |GTH| = \dfrac{|Y_2/Y_1|}{|G_{TC}|} \\ \Phi(GTH) = -180^\circ + \Phi\left(\dfrac{Y_2}{Y_1}\right) - \Phi(G_{TC}) \end{cases} . \quad (2)$$

A temporary PI compensation controller, G_{CT}, with transfer function $6(1 + (1/63s))$ was utilized in the closed-loop frequency response measurement in order to control the thermal system around the desired temperature set point. Fig. 3 shows the measured closed-loop frequency response, Y_2/Y_1. Due to the limited minimum frequency of the 35670A for a swept sine signal, we could only perform frequency response measurements down to 0.015625 Hz. However, this proved to be low enough for us to design the controller. The open-loop transfer function of the thermal system calculated from Eq. (2) is plotted in Fig. 4.

From the figure note the 0.025 Hz phase-crossover frequency. This is much slower than the ~10 s air change-over time or the

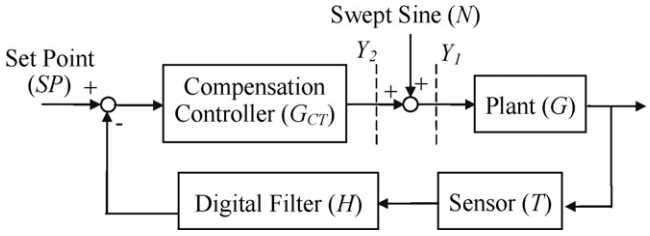

Fig. 2. Thermal system control diagram including measurement points for determining the closed-loop frequency response.

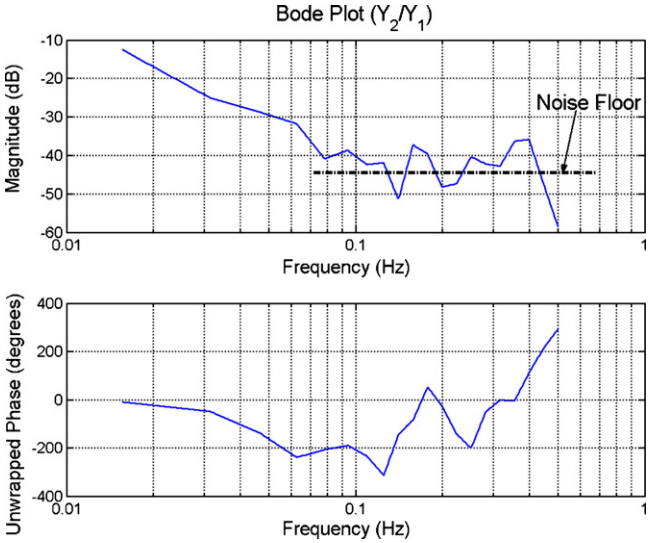

Fig. 3. Bode plot of measured system closed-loop frequency response, Y_2/Y_1.

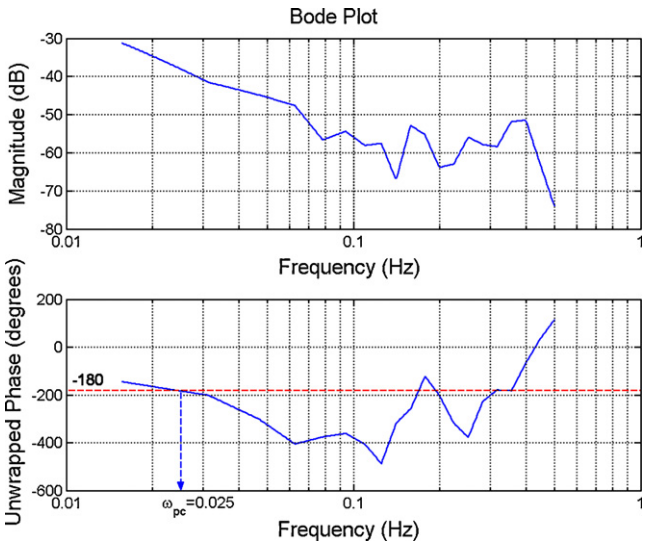

Fig. 4. Bode plot of measured open-loop transfer function for the thermal system. ω_{pc} is the phase-crossover frequency.

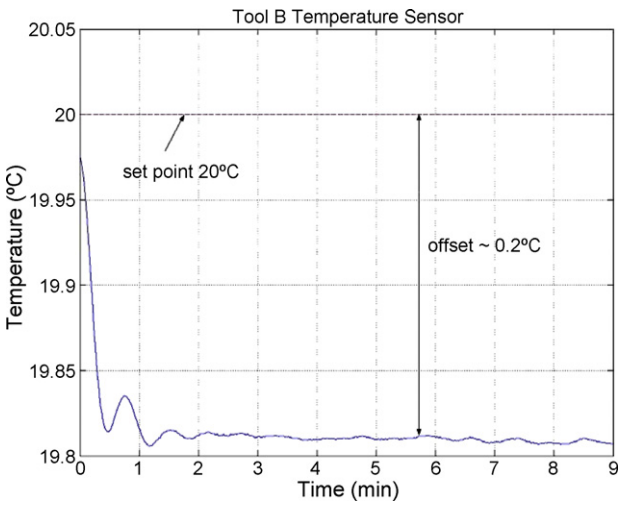

Fig. 6. Measured performance of the thermal control system without the PI controller. The thermal controller was turned on at time 0.

~1 s fast heater response time and is dominated by the ~1.5 min response time of the system's control thermistors.

3. Controller design

Based on the measured transfer function of the thermal system, we designed a lead compensation controller with transfer function $(100s+1)/(15s+1)$, which reduced overshoot by increasing the phase margin and resulted in a faster transient response by increasing the phase-crossover frequency to 0.035 Hz. Bode plots of the open-loop transfer functions for the lead-compensated system and uncompensated system are shown in Fig. 5.

A PI controller with transfer function $1+(1/1000)(1/s)$ was also added into the control system in order to eliminate the steady-state error. Fig. 6 shows a measured steady-state error of around 0.2 °C with respect to the set point (20 °C) when there is no PI controller.

Fig. 7 shows a diagram of our complete thermal control system. The s-domain system design (Fig. 7a) was converted to a z-domain

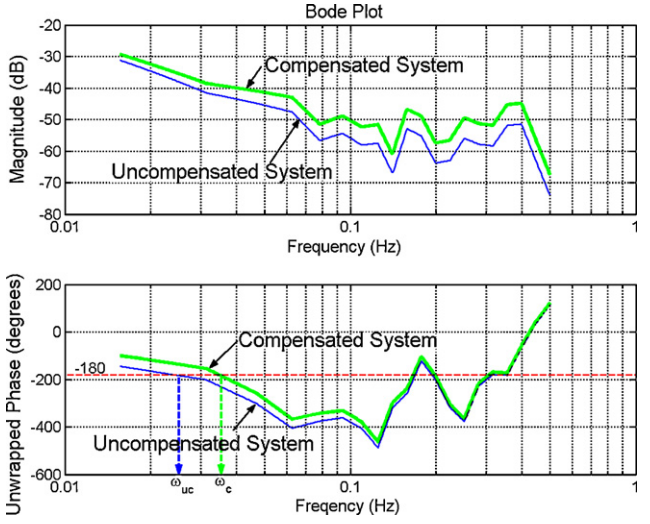

Fig. 5. Measured Bode plots of the open-loop transfer function for the lead-compensated and uncompensated system. ω_{uc} is the phase-crossover frequency of the uncompensated system and ω_c is the phase-crossover frequency of the compensated system.

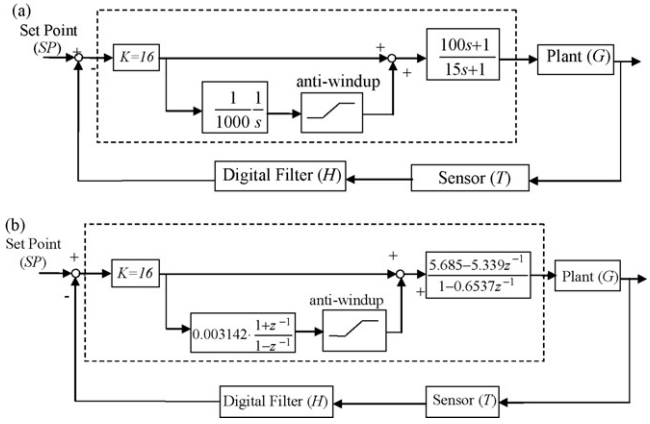

Fig. 7. Diagram of the complete thermal control system. The portion inside the dashed area represents the digital controller. (a) The controller in s-domain. (b) The controller in z-domain.

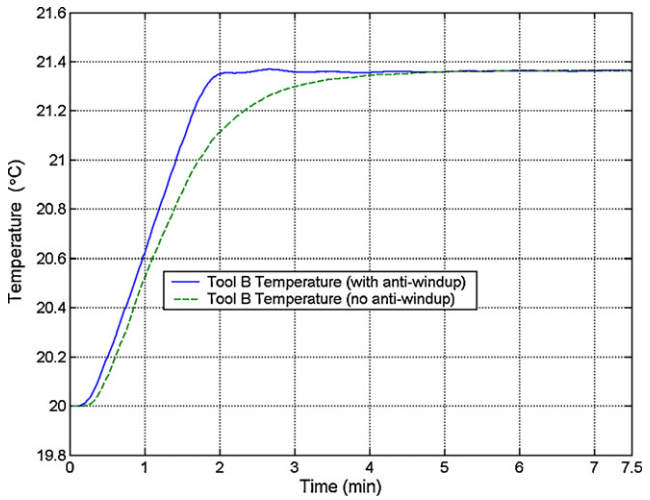

Fig. 8. Measured thermal system responses to a step input of the set point.

design (Fig. 7b) using a bilinear approximation and implemented in a MicroLogix™ 1200 programmable logic controller, with a cycle speed of 1 Hz. In Fig. 7a and b the digital controller is enclosed by a dashed box. A digital filter, H, is utilized to reduce the measurement noise of the system thermistors by averaging 1-s of thermistor measurements (approximately 50–100 data points). The averaging shrinks the measurement noise from 2–3 to 0.3 m°C. We set the gain, K, to 16, which was selected to achieve an optimal transient response to a step input of the set point. An anti-windup block was utilized to avoid the effect of integrator windup [9], which reduces the transient response time and speeds up temperature recovery from large thermal disturbances, for example, after opening the enclosure door. Fig. 8 shows the system response to a step input of the set point. The system with the anti-windup block will reach the new set point much more quickly than without anti-windup block. For example, after briefly opening the enclosure door to change lithography substrates, the system will recover within 3 min to within ±0.002 °C of the set point.

4. Performance of the thermal control system

With the PI-lead compensation controller, a single-point air temperature stability of less than 1 m°C, one-sigma, was obtained during a 2-h interval, which is shown in Fig. 9. The feedback temperature sensor of the thermal control system measured a one-sigma stability of 0.7 m°C and independent temperature sensor obtained a one-sigma stability of 0.5 m°C. The difference in performance as measured by the system sensor and the independent sensor is due to their different response times (see section below).

Before the improvements to the thermal control system, the system sensor measured a 2.4 m°C one-sigma air temperature stability at a single point over a 2 h interval. The performance of the thermal control system before and after the improvements is shown in Fig. 10. All temperature measurements were sampled at 1 Hz.

5. Thermistor cross calibration and the self-heating effect

Independent temperature measuring system (Instrulab Model 3312A 12-channel thermometer) was utilized to map temperature gradients and test the performance of the thermal control system. Details of our thermal calibration and mapping experiments can be found in Ref. [10]. The temperature data acquisition system has a stated accuracy of 10 m°C and a resolution of 1 m°C. We confirmed the system noise to be less than 1 m°C. The system uses model 052SS sensors which are 4-wire water-proof themistors with a 3-min time constant in air. Data sampling rate is 0.25 Hz.

Accurate cross calibration of the thermistors is important in order to obtain sub-millidegree-relative-accuracy temperature gradient maps. Some water baths can provide a temperature stability of ±25 μ°C over 24 h [11]. Here a simple calibration water bath shown in Fig. 11 was constructed from a glass beaker equipped a standard lab electro-magnetic stirring rod which was covered with insulation foam and placed inside the environmental enclosure, resulting in a temperature gradient of less than 1 m°C. Temperature measurements of 11 thermistor channels immersed in the calibration bath are shown in Fig. 12. The measurement of each thermistor over 9 h varied within 1 m°C.

Based on the difference between the mean of each thermistor's measurement to the average of the means of all 11 thermistors, both measured over 9 h, the offset for each thermistor was determined to provide an accurate cross-calibration. The formal uncertainty of the corrections is of ±0.004 mC, which is much less than the LSB of the temperature readout. The corrections were all very small – within ±1.1 mC – indicating that the manufacturer had done a good calibration job at the factory.

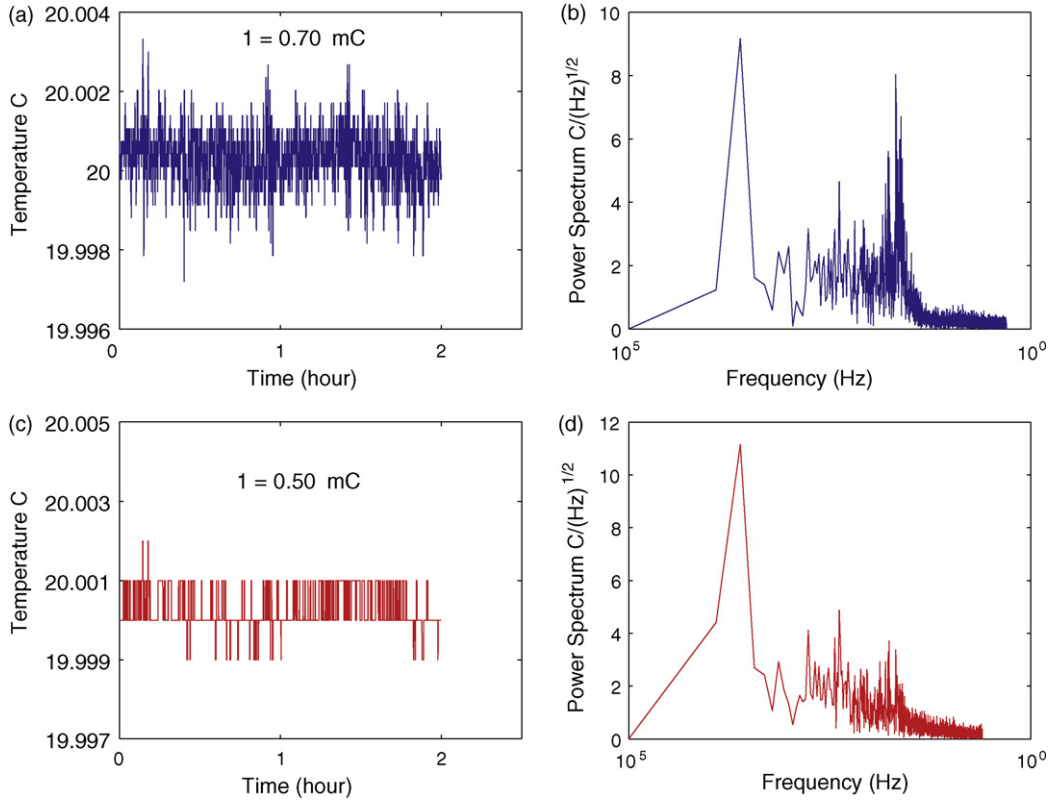

Fig. 9. Two hours of single-point temperature measurements of the thermal system. (a) Measured side B temperature with the system sensor. (b) Frequency content of measured side B temperature with the system sensor. (c) Measured side B temperature with an independent sensor. (b) Frequency content of measured side B temperature with the independent sensor.

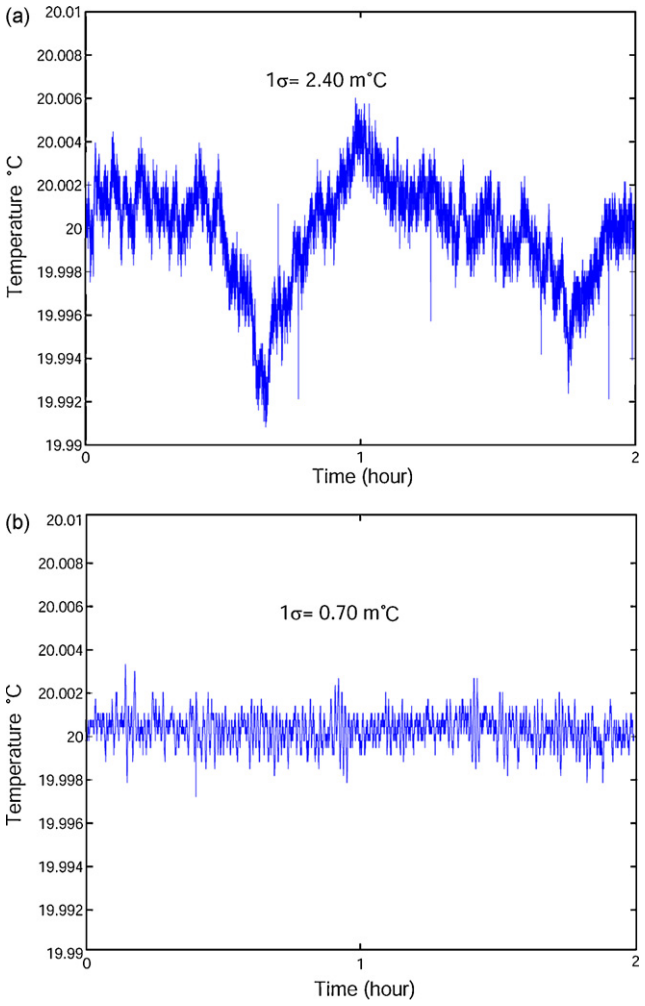

Fig. 10. Two hours of single-point side B temperature measurements of the thermal system with the system sensor. (a) Before the improvement of the thermal control. (b) After the improvement of the thermal control.

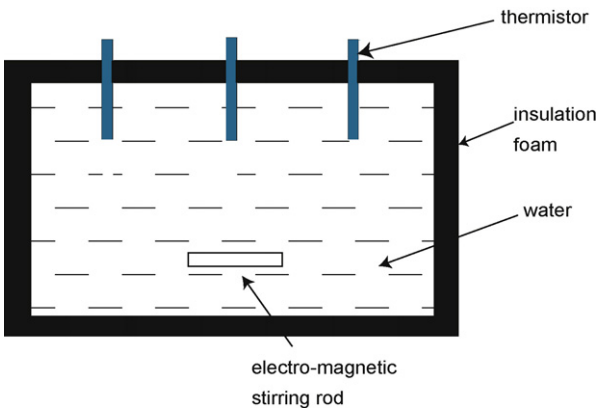

Fig. 11. Schematic of calibration water bath.

The self-heating effect of thermistors may potentially cause incorrect measurements when thermistors traverse regions of changing wind velocity (1–2 m/s) [12,13]. The excitation current of the Instrulab 3312A is about 80 μA which generates a heat pulse of 3.5 μJ in each thermistor during the 0.3-s measurement. Based on a simple heat capacity calculation, the uncertainty due to self-heating is <70 μ°C. The fact that the self-heating effect on temperature measurement in winds of 1–2 m/s is less than 1 m°C was also verified in an experiment that compared the temperature measurements of an instantaneous turn-on thermistor channel and a reference thermistor channel.

6. Mapping millidegree temperature gradients

Monitoring and mapping temperature gradients over large volumes is usually limited by the number of the thermistors and thermistor placement. We constructed a simple aluminum-rod frame for our study to rapidly position thermistors in space. Eight thermistors were attached by high-thermal-impedance mounts to a vertical rod in this frame, which can be mechanically scanned in

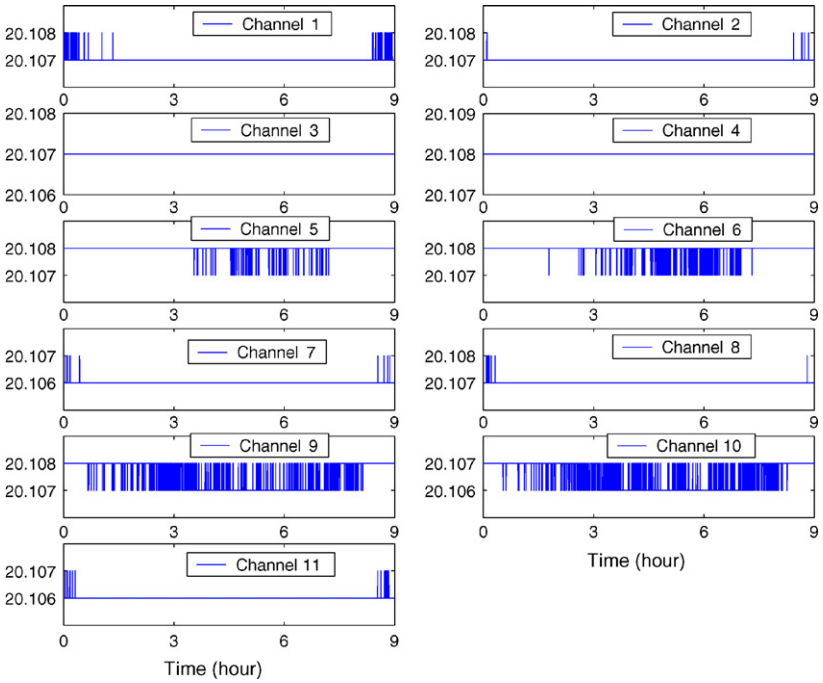

Fig. 12. Temperature measurements of 11 thermistor channels (°C) over 9 h in the thermal calibration bath.

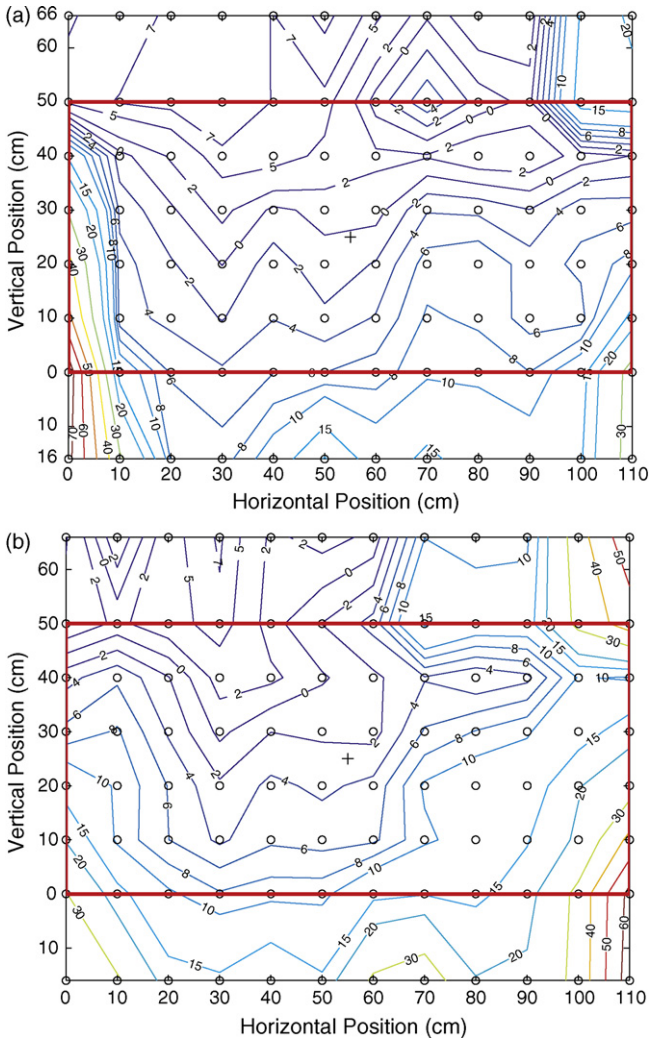

Fig. 13. Contour plots of relative temperatures (m°C) over an area 30 cm from the filter plane of air handler B. (a) Before the improvement of the single-point thermal control. (b) After the improvement of the single-point thermal control. The central rectangle represents the filter boundary, the circles represent the thermistor measurement positions, and the central cross represents the reference thermistor.

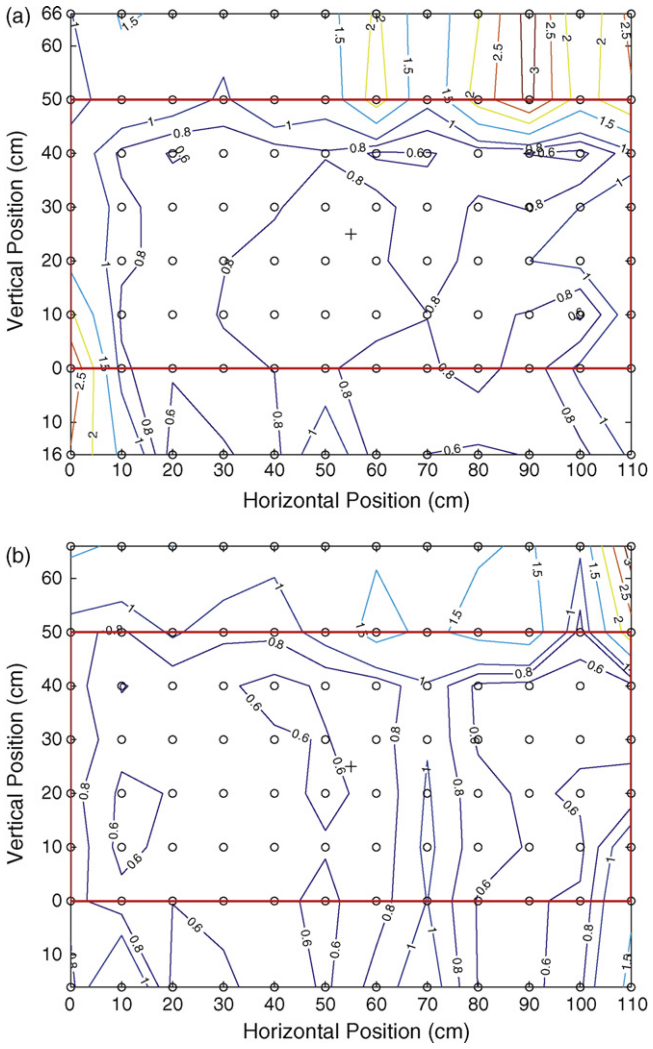

Fig. 14. Standard deviation maps of temperatures (m°C) over an area 30 cm from the filter plane of air handler. (a) Before the improvement of the single-point thermal control. (b) After the improvement of the single-point thermal control. The central rectangle represents the filter boundary, the circles represent the thermistor measurement positions, and the central cross represents the reference thermistor.

a horizontal direction by an external string, and thus used to map temperature gradients within the mapping plane, as shown by the rectangle in Fig. 1a. Note the vertical placement of thermistors on the rod, which are spaced at 10 cm intervals within the filter plane, can be discerned by looking at the location of the open circles in Fig. 13.

A stationary thermistor placed at the filter plane center was utilized as a reference in order to eliminate the effect of temperature variations during mapping. By always referencing temperatures, measured as a function of time, to the temperature at the map's center helps reduce errors due to temperature fluctuations and helps to see small and persistent temperature gradients across the measurement volume. In practice, however, since temperature fluctuations are generally small (~1 mC) in our system compared to the temperature gradients, use of a center reference makes only a modest reduction in mapping errors.

During the mapping process, we move the vertical rod from outside the enclosure, avoiding the large thermal disturbances due to opening and entering the enclosure and significantly reducing the mapping time. We stopped the vertical rod at 12 horizontal locations in sequence. At each location the eight thermistors took 15 min of measurements. We utilized only the last 8 min of data to generate maps since there is a several-minute transient time due to rod movement. It takes only 3 h to map a 110 cm × 82 cm area, which is much more rapid than the case of opening the enclosure and relocating the thermistors by hand. At each measurement point, the mean of the relative temperature of this point with respect to the temperature at the center of the filter plane, averaged over 8 min, is calculated in order to generate a relative temperature map. The standard deviation of this relative temperature is also plotted. Fig. 13 shows the relative temperature gradients over a 110 cm × 82 cm area which is 30 cm away from the ULPA filter plane of the air handler B, measured before and after the improvement of the thermal control. The corresponding standard deviation maps are shown in Fig. 14. In main areas of the mapping plane the relative temperature gradients are within 10 m°C and their corresponding standard deviation is no more than 1 m°C. The improvement of the single-point thermal control also improved the temperature stability over the mapped area, but did not dramatically change the temperature gradients within the same area.

7. Conclusions and discussion

In this study, we presented a method to measure the open-loop transfer function of a thermal system. Based on the measured transfer function, we designed a lead compensation controller together with a PI controller for the thermal control of an environmental enclosure. Sub-millidegree air temperature stability for a large-volume enclosure has been achieved. A method to rapidly monitor and map millidegree temperature gradients over large volumes of enclosed space by mechanically scanning a network of thermistors has been developed and the temperature gradients within the critical tool volumes have been measured. Accurate cross calibration (within 1 m°C) of the thermistors has been performed. Self-heating errors have been shown to be less than 1 m°C. Sub-millidegree-relative-accuracy temperature gradients maps have been utilized to test the enclosure thermal system improvements.

Further improvement of thermal control could perhaps be achieved by use of control sensors with lower noise and a faster response time. The 0.02 Hz noise peak in the power spectrum (see Fig. 9), which lies just at the edge of the system's useful control bandwidth, could probably be reduced further with this improvement. While we achieved dramatic improvements in single point temperature stability, the persistent temperature gradients in the air-flow are a concern. Considering only the central 30 cm × 90 cm of the filter plane, gradients of up to 25 m°C were observed (see Fig. 13). These hot spots could cause large interferometer errors if this laminar air becomes turbulently mixed downstream and gets into the beam paths, which is likely the case for our lithography tool, especially during stage motion. The origin of the temperature gradients is not known. Further improvements in this area could perhaps be achieved by use of improved air mixing and ducting with better thermal insulation. Special ducts which direct air to the interferometer beams (also known as air showers) could also potentially reduce turbulent mixing and further reduce interferometer noise.

Acknowledgements

The authors gratefully acknowledge the assistance of Robert Fleming from the MIT Space Nanotechnology Laboratory. This research is supported by the National Science Foundation under the Nanoscale Interdisciplinary Research Team (NIRT) Grant DMI-0506898.

References

[1] Brich KP, Downs MJ. Correction to the updated Edlen equation for the refractive index of air. Metrologia 1994;30:315–6.
[2] Sarid D, Cannell DS. A ±15 microdegree temperature controller. Review of Scientific Instruments 1974;45:1082–8.
[3] Dratler J. A proportional thermostat with 10 microdegree stability. Review of Scientific Instruments 1974;45:1435–44.
[4] Ogasawara H. Method of precision temperature control using flowing water. Review of Scientific Instruments 1986;57:3048–52.
[5] Lawton KM, Patterson SR. A high stability air temperature control system. Precision Engineering 2000;24:174–82.
[6] Konkola PT. Design and analysis of a scanning beam interference lithography system for the patterning gratings with nanometer-level distortions, Ph.D. dissertation, Massachusetts Institute of Technology, Department of Mechanical Engineering, June; 2003.
[7] Konkola PT, Chen CG, Heilmann RK, Joo C, Montoya JC, Chang C-H, et al. Nanometer-level repeatable metrology using the Nanoruler. Journal of Vacuum Science & Technology B 2003;21(6):3097–101.
[8] Heilmann RK, Chen CG, Konkola PT, Schattenburg ML. Dimensional metrology for nanometer-scale science and engineering: towards sub-nanometer accurate encoders. Nanotechnology 2004;15:S504–11.
[9] Karl J, Astrom, Bjorn Wittenmark. Computer-controlled systems: theory and design. 3rd ed. Prentice Hall; 1996.
[10] Zhao Y. Ultra-high precision scanning beam interference lithography and its application—spatial frequency multiplication, Ph.D. dissertation. Massachusetts Institute of Technology, Department of Mechanical Engineering, May; 2008.
[11] Harvey ME. Precision temperature-controlled water bath. Review of Scientific Instruments 1968;39(1):13–8.
[12] Lawton KM, Patterson SR. Long-term relative stability of thermistors. Precision Engineering 2001;25:24–8.
[13] Lawton KM, Patterson SR. Long-term relative stability of thermistors: part 2. Precision Engineering 2002;26:340–5.